

# Microkinetic interpretation of HDS/HYDO selectivity of the transformation of a model FCC gasoline over transition metal sulfides

A. Daudin<sup>a,c</sup>, A.F. Lamic<sup>a</sup>, G. Pérot<sup>a</sup>, S. Brunet<sup>a,\*</sup>, P. Raybaud<sup>b,c</sup>, C. Bouchy<sup>c</sup>

<sup>a</sup> UMR CNRS 6503, Catalyse en Chimie Organique, Université de Poitiers, Faculté des Sciences Fondamentales et Appliquées, 40 Avenue du Recteur Pineau, 86022 Poitiers Cedex, France

<sup>b</sup> IFP, Direction Chimie et Physico-Chimie Appliquées, 1-4 Av. de Bois Préau, 92858 Rueil Malmaison, France

<sup>c</sup> IFP-Lyon, Direction Catalyse et Séparation, BP 3, 69390 Vernaison, France

Available online 12 September 2007

## Abstract

The conversion of a model FCC gasoline (composed of 2-methylthiophene (2MT), 2,3-dimethylbut-2-ene (23DMDB2N) and orthoxylene in *n*-heptane) under realistic hydrodesulfurization (HDS) conditions was investigated over a serie transition monometallic sulfides (Ni<sub>3</sub>S<sub>2</sub>, PdS, Co<sub>9</sub>S<sub>8</sub>, Rh<sub>2</sub>S<sub>3</sub>, RuS<sub>2</sub>, PtS and MoS<sub>2</sub>) and unsupported transition bimetallic sulfide catalysts (NiMoS and CoMoS). The results reveal for the first time that a volcano curve relationship exists between the ab initio calculated sulfur–metal bond energy,  $E(\text{MS})$ , descriptor of bulk TMS and their activities in olefin hydrogenation and in alkylthiophene desulfurization measured simultaneously. In particular, Rh<sub>2</sub>S<sub>3</sub> with an intermediate sulfur–metal bond energy of 119 kJ/mol is the most active catalyst in both case hydrogenation of the olefin and in HDS of a sulfur compound. Furthermore, the HDS/HYDO selectivity which is the most important parameter in the deep HDS of gasoline, presents a maximum for the NiMoS catalyst with  $E(\text{MS})$  of 128 kJ/mol. A microkinetic model based on Brønsted–Evans–Polanyi relationships and the competitive adsorption of the sulfur molecule and alkene on the catalytic site is proposed to give a rational interpretation of the experimental catalytic results.

© 2007 Elsevier B.V. All rights reserved.

**Keywords:** Hydrogenation; Hydrodesulfurization; Gasoline; Transition metallic sulfide catalysts; 2,3-Dimethylbut-2-ene; 2-Methylthiophene; Microkinetic

## 1. Introduction

The reduction of the sulfur level in diesel and gasoline down to 10 wt ppm planned for 2009 in the European Union [1] will require the elaboration of new catalysts or the optimization of conventional catalysts. The gas emission from motor vehicles (NO<sub>x</sub> and SO<sub>x</sub>) contributes widely to air pollution and sulfur is a well-known poison for catalytic converters. The gasoline fraction produced from the FCC process represents 30–50% of the commercialized motor fuel but it contains up to 85–95% of the sulfur impurities. It is mainly composed of aromatics (30 vol%), *iso*-alkenes (30 vol%) and sulfur compounds such as alkylthiophenes (maximum 5000 ppm) [2–4]. A high hydro-treating selectivity, corresponding to a high HDS activity and a

low hydrogenation activity for olefins (HYDO) is required. Indeed, significant alkene saturation can occur during the HDS process, which leads to a decrease of the octane number in the final product. Consequently, hydrotreating catalysts must meet selective criteria HDS/HYDO, i.e. achieve a deep HDS with minimum olefin saturation.

Recent works [5,6] showed that the isomerization step could be a key factor in the hydrogenation of alkenes. Indeed, Mey et al. [6] showed that the first step for the transformation of 23DMDB2N was its isomerization in 23DMDB1N followed by the hydrogenation step to produce 23DMB.

The HDS/HYDO selectivity was increased by modifying the acid–base properties of the support, on one hand, by decreasing the acidity of the support by alkaline elements (e.g. Li, K) [6–8] or by using a more basic support such as hydrotalcite [9], on the other hand, by poisoning selectively hydrogenation sites by carbon deposition [10,11] or adsorption of basic nitrogen compounds [12]. Indeed, Mey et al. [6] have shown a decrease

\* Corresponding author. Tel.: +33 549453627; fax: +33 549453897.

E-mail address: [sylvette.brunet@univ-poitiers.fr](mailto:sylvette.brunet@univ-poitiers.fr) (S. Brunet).

in the hydrogenation activity on CoMo supported catalyst modified by potassium. These results have been explained by the inhibition of the olefin isomerization activity and consequently the activity of the catalyst in olefin hydrogenation decreased.

Transition metal sulfide (TMS) catalysts are known to be active in the various hydrotreating reactions [13]. Pecoraro and Chianelli [14] were the first to report a systematic study of the intrinsic activity of bulk monometallic transition metal sulfides (TMS) in a model reaction, the hydrodesulfurization (HDS) of dibenzothiophene at 400 °C. They established a relative activity scale for TMS as a function of the periodic position of the transition metals. These results were further confirmed by several experimental studies either for unsupported or supported sulfides in HDS, hydrodenitrogenation (HDN) and hydrogenation of aromatics (HYD) [14–17].

Advances in molecular modeling at the density functional theory (DFT) level and realistic models of sulfide catalysts have enabled the finding of quantitative structure activity relationship (QSAR) valid for numerous TMS [18–21] which are referred as “volcano curve” relationship. In particular, the descriptor used for such QSAR approach is defined as the bulk sulfur–metal bond energy  $E(\text{MS})$  of the TMS and shows in evidence how experimental activity patterns can be correlated to computed-bond-energy descriptor in accordance with the Sabatier principle [22]. It has been established that volcano type relationships between the *ab initio* calculated sulfur–metal bond energies  $E(\text{MS})$  and various catalytic activities relevant for hydrotreatment processes: HDS of dibenzothiophene [23], HYD of biphenyl [18,24] and toluene [25,26] and more recently HYD of olefins [27].

According to our knowledge, the correlation between the activities of TMS and their corresponding  $E(\text{MS})$  descriptor has not been yet investigated for the transformation of a model FCC gasoline. Hence, the purpose of this paper is to evaluate the activity of various unsupported TMS ( $\text{Ni}_3\text{S}_2$ , PdS,  $\text{Co}_9\text{S}_8$ ,  $\text{Rh}_2\text{S}_3$ ,  $\text{RuS}_2$ , PtS,  $\text{MoS}_2$ , CoMoS and NiMoS) catalysts in the transformation of a model feed composed of 2,3-dimethylbut-2-ene (23DMB2N) 20 wt%, 2-methylthiophene (2MT) and orthoxylene (30 wt%), in *n*-heptane. The alkene and sulfur compounds were considered, respectively, as representatives of olefins and sulfur molecules found in FCC gasoline. TMS were chosen in order to cover a representative scale of sulfur–metal bond energies,  $E(\text{MS})$  as defined in ref. [23]. Unsupported TMS were used for this study in order to avoid any possible support effect. The reactivity of the model feed was measured under typical condition used for selective HDS of FCC gasoline. Hydrogenation and hydrodesulfurization activities as regard to the tested TMS are discussed with the  $E(\text{MS})$  descriptor calculated by Toulhoat and Raybaud [23] in order to explore if volcano curves may exist for the two model reactions (hydrogenation and hydrodesulfurization in competition). Furthermore, in the case of 23DMB2N hydrogenation and 2MT hydrodesulfurization, we propose a microkinetic model to explain the  $E(\text{MS})$ –activity relationships obtained.

## 2. Experimental

### 2.1. Catalyst preparations

Co, Ni, Ru, Rh, Pd and Pt sulfides were prepared by using the non-aqueous precipitation method reported by Pecoraro and Chianelli [14]. The metal chloride precursor and lithium sulfide were added in ethyl acetate and the metal sulfide was obtained after 4 h of stirring at 80 °C. Then, the solution was cooled down to room temperature, filtrated in order to recover the dark precipitate. The corresponding sulfide solid was stabilized by a first sulfidation step in  $\text{H}_2/\text{H}_2\text{S}$  (10 mol%  $\text{H}_2\text{S}$ ) flow during 2 h at 400 °C (heating rate: 3.3 °C/min). LiCl was removed by several washes with acetic acid and vacuum filtration. Finally, the metallic sulfide was obtained after a second sulfidation procedure under usual conditions.

Molybdenum sulfide preparation was carried out by thermal decomposition of ammonium thiomolybdate [28,29] at 400 °C under  $\text{H}_2/\text{H}_2\text{S}$  (10%  $\text{H}_2\text{S}$ ) flow during 4 h. First, the ammonium tetrathiomolybdate  $(\text{NH}_4)_2\text{MoS}_4$  (ATM) was obtained by reaction between ammonium heptamolybdate  $(\text{NH}_4)_6[\text{Mo}_7\text{O}_{24}]\cdot 4\text{H}_2\text{O}$  (4 g in 20 cm<sup>3</sup> of distilled water) with a 50 wt% of ammonium sulfide  $(\text{NH}_4)_2\text{S}$  in aqueous solution at 60 °C. The ATM precursor precipitated as red crystals by cooling down the solution in iced water during 3 h. Then, the precipitated red crystals were thoroughly washed with isopropanol and dried.

Molybdenum based catalyst promoted by nickel or cobalt to obtain NiMoS and CoMoS catalysts were prepared according to the method reported by Fuentes et al. [30].  $(\text{NH}_4)_2\text{MoS}_4$  (prepared as mentioned below) was used as a support to impregnate  $\text{Co}(\text{NO}_3)_2$  or  $\text{Ni}(\text{NO}_3)_2$  diluted in acetone in order to obtain atomic ratio of  $\text{Ni}(\text{Co})/(\text{Ni}(\text{Co}) + \text{Mo}) = 0.3$ . The bimetallic organosulfides precursors were obtained by removing the solvent at room temperature. Finally, NiMoS and CoMoS catalysts were prepared by thermal decomposition of the corresponding bimetallic organosulfide precursor at 400 °C under  $\text{H}_2/\text{H}_2\text{S}$  (10%  $\text{H}_2\text{S}$ ) flow during 4 h.

### 2.2. Characterization

TMS were characterized before and after catalytic activity measurements by TEM combined with EDX (Philips CM 120 kV), X-ray diffractions (Bruker D5005), BET surface area (Micromeritics ASAP 2010) and elemental analysis (CE Instruments NA2100 Protein) at the University of Poitiers (LACCO) in order to verify the exact nature of TMS and that there was no modification of the catalyst during the test. Comparison between XRD patterns and JCPDS database allowed the identification of the various crystalline TMS phases.

XPS spectra were recorded using a KRATOS AXIS Ultra spectrometer equipped with a 300 W Al K $\alpha$  source ( $h\nu = 1486.6$  eV). TMS samples were packed in shlenk under argon to avoid sulfate formation. They were identified with reference samples drawn from the Handbook of X-ray photoelectron spectroscopy [31], NIST X-ray Photoelectron Spectroscopy Database (NIST Standard Reference Database 20, Web Version 3.4).

The calibration has been made with the carbon peak of contamination identified at 284 eV. For each TMS, the metal and sulfur peaks have been identified with their binding energies. The elemental surface composition of the TMS and therefore the atomic ratio of sulfur/metal (S/Me) after reaction were determined from the intensity of the metal and sulfur peaks (relative measuring error around 20%).

### 2.3. Reaction conditions

Catalytic activity measurements were carried out in a fixed-bed reactor at 250 °C under a total pressure of 20 bar. The catalyst was sulfided at 400 °C for 10 h with a mixture of 10 mol% H<sub>2</sub>S in H<sub>2</sub> under atmospheric pressure and then cooled down to the reaction temperature in the presence of the sulfiding mixture. The desired reaction conditions were adjusted, then the model feed was injected into the reactor. The model feed was composed of 0.3 wt% (1000 ppm S) of 2MT, 20 wt% of 23DMB2N, 30 wt% of orthoxylene and 49.7 wt% of *n*-heptane. The residence time varied from 2 to 324 s corresponding to LHSV from 0.7 to 9.2 h<sup>-1</sup>. The ratio H<sub>2</sub>/feed was equal to 360 l/l.

All partial pressures conditions of the various components for sulfidation step and catalytic activity measurements are reported in Table 1.

### 2.4. Analysis of HYDO and HDS products

The reaction products were injected on-line by means of an automatic sampling valve into a Varian gas chromatograph equipped with a PONA capillary column, a flame ionization detector and a cryogenic system.


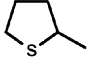
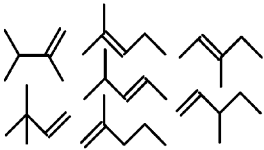
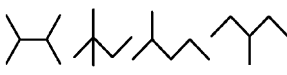
The identification of the products was performed by GC–MS coupling (Table 2). No significant transformation of orthoxylene was observed, whatever the experimental conditions. For both 2MT and 23DMB2N transformation, the same products were detected over the various TMS catalysts as those observed over the conventional CoMo/Al<sub>2</sub>O<sub>3</sub> catalyst [5,6].

Desulfurized products, resulting from the transformation of 2-methylthiophene were designated as HDS products. The selectivity of the reaction is given by the ratio between hydrodesulfurization and olefin hydrogenation (HDS/HYDO).

HDS and HYDO activities per unit surface area of the TMS catalysts were measured after stabilization from, respectively,

Table 2

Products resulting from the transformation of model compounds

Transformation of 2-methylthiophene (2MT)		
HDS	 C <sub>3</sub> , C <sub>3</sub> , C <sub>4</sub>	2-methyltetrahydrothiophene (2MTHT) 
Transformation of 2,3-dimethylbut-2-ene (23DMB2N)		
Isomerization		Hydrogenation (HYDO)
		

HDS and HYDO products formation and under conditions where a linear relationship between conversion and residence time was obtained (the yield in HDS was around 40% and the yield in hydrogenation products around of 15%).

The transformation of the 2,3-dimethylbut-2-ene (23DMB2N) led to the formation of isomerization products (mainly 2,3-dimethylbut-1-ene, 23DMB1N) and hydrogenation products (mainly 2,3-dimethylbutane, 23DMB) (Scheme 1). Thiols, which could be resulting from reaction of H<sub>2</sub>S and olefins (23DMB2N and 23DMB1N), were not observed under our experimental conditions. It should be emphasized that the limit of detection for such compounds was estimated to ca. 10 ppm wt with the GC analysis. The isomerization between 23DMB2N and its isomer (23DMB1N) was very fast. In fact, the equilibrium mixture of both isomers was considered as the reactant [5,32]. The hydrogenation activity was measured with the formation of 23DMB which was the main hydrogenation product. Skeletal isomers and their hydrogenation products were obtained with a yield of less than 1%.

Regarding the transformation of the 2-methylthiophene, HDS products (mainly pentanes and pentenes) were the main products according to the reaction scheme described in the literature [6,13] (Scheme 2).

### 2.5. Microkinetic modeling

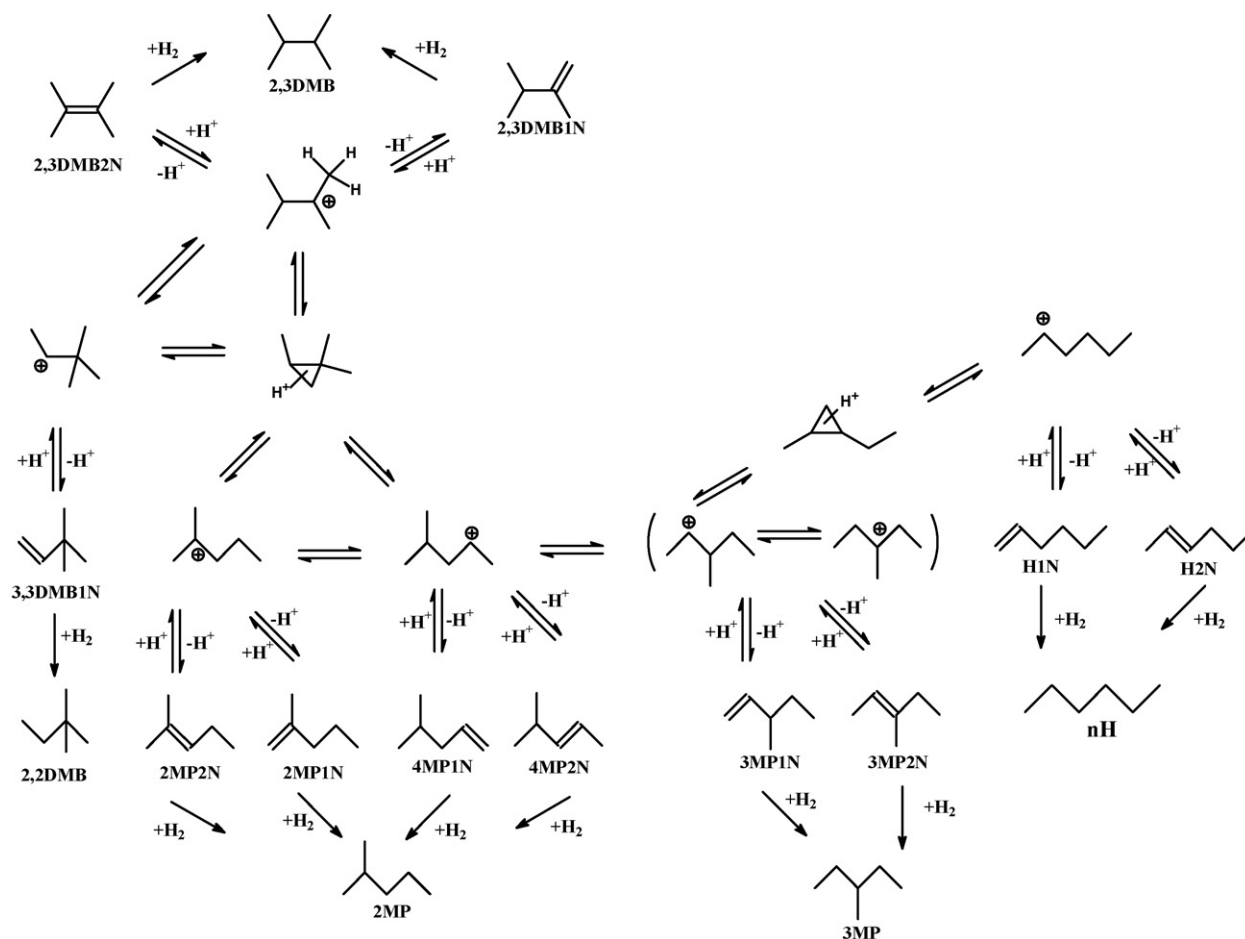
Previous works have successfully combined sulfur–metal bond descriptor and microkinetic modelling within the Langmuir–Hinshelwood formalism for some reactions over sulfide catalysts such as HYD of aromatics (biphenyl, toluene) [18,25,26] and HDS of dibenzothiophene [23].

These results suggest a general interpretation of periodic trends in catalysis by sulfides for various types of reaction. In the same spirit, we have determined the best model able to reproduce experimental catalytic results obtained for HDS of 2MT and HYD of 23DMB2N considering both reaction simultaneously in order to take into account the competitive adsorption effect between both compounds on the same active site.

Table 1

Partial pressures of the different components for the preliminary sulfidation step and the transformation of the model feed

Pressure (bar)	Sulfidation	Feed
<i>P</i> <sub>olefin</sub>	0	2.27
<i>P</i> <sub>H<sub>2</sub>S</sub>	0.1	0
<i>P</i> <sub>2MT</sub>	0	0.03
<i>P</i> <sub>o-xyl</sub>	0	2.69
<i>P</i> <sub>H<sub>2</sub></sub>	0.9	10.28
<i>P</i> <sub>nC7</sub>	0	4.73
<i>P</i> <sub>total</sub>	1	20



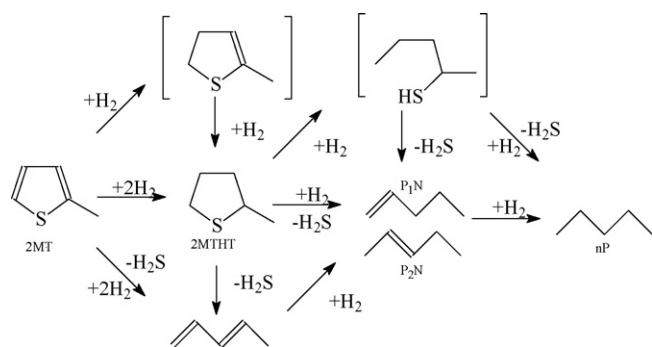
Scheme 1. 23DMB2N transformation, isomerization and hydrogenation products. 23DMB2N, 2,3-Dimethylbut-2-ene; 23DMB1N, 2,3-dimethylbut-1-ene; 33DMB1N, 3,3-dimethylbut-1-ene; 2MP1N, 2-methylpent-1-ene; 2MP2N, 2-methylpent-2-ene; 4MP1N, 4-methylpent-1-ene; 4MP2N, 4-methylpent-2-ene; 3MP1N, 3-methylpent-1-ene; 3MP2N, 3-methylpent-2-ene; 22DMB, 2,2-dimethylbutane; 2MP, 2-methylpentane; 3MP, 3-methylpentane ([6]).

On the basis of earlier works of Kasztelan et al. [33,34] the model proposed in the present work is a one site model with dissociative adsorption of  $\text{H}_2\text{S}$  and  $\text{H}_2$  at the catalyst surface. Thus, the sulfydryl group engendered by  $\text{H}_2\text{S}$  dissociation take part to the elementary step of the reaction. In what follows, we will focus on this microkinetic model proposed for both reaction: 23DMB2N hydrogenation and methylthiophene HDS. This model is optimized by expressing the adsorption constants and activation energies as a linear relationship of the

sulfur–metal bond energies calculated by DFT previous work [20,21,23].

#### 2.5.1. Elementary step of the HYD and HDS mechanisms

First, Eqs. (E1)–(E7) describe the relevant elementary steps of the mechanism involved in the one site ( $\text{M}^*$ ) microkinetic model of 23DMB2N hydrogenation:



Scheme 2. Formation of the HDS products from 2MT. 2MT, 2-methylthiophene; 2MTHT, 2-methyltetrahydrothiophene; P1N, pent-1-ene; P2N, pent-2-ene; nP, n-pentane.

Step (E0) corresponds to the creation of MS species, from the  $\text{M}^*$  site, which is directly related to the sulfidation equilibrium



state of the catalytic surface depending on the sulfo-reductive conditions as revealed by DFT calculation [35]. Even if it can not be rigorously regarded as an elementary step of the reaction, the experimental conditions ( $T$  and  $P_{H_2S}/P_{H_2}$ ) may change the surface chemical state and the distribution of MS and  $M^*$  species. In addition, the distribution of MS and  $M^*$  species is also influenced by the elementary steps of the reaction (E1)–(E6).

At the same time, equation (E0) assuming a link between MS and  $M^*$  avoids to consider a more complex model with two independent sites. Indeed, we have also tested a two sites model. Even if such a model offers more degrees of freedom to fit with experiments, the larger number of fitted parameters makes difficult to validate the final solution in absence of more experimental data. In addition, no significant improvement was obtained with the best fitted two sites model. Thus, the one site model is chosen as a good compromise.

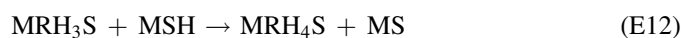
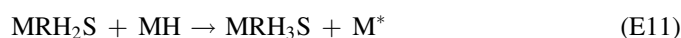
$H_2$  and  $H_2S$  are both activated through dissociation steps (E1) and (E2). Although this model does not require to explicitly represent the charges of the species, these two dissociation steps can be formally considered as heterolytic because of the nucleophilic character of MS species and electrophilic character of  $M^*$ , leading to a charge redistribution during the H–H splitting. Olefin adsorption (labelled as R) is reported at step (E3). For the optimal model described here, step (E4) is assumed to be rate determining and correspond to the first hydrogen transfer from the sulfhydryl group to the adsorbed olefin. Step (E5) is the second hydrogen transfer from a MH species. Finally, step (E6) corresponding to alkane desorption with simultaneous regeneration of  $M^*$  sites.

In order to equilibrate the global reaction scheme, the following final step is proposed:



Step (E7) shows in evidence that  $H_2S$  takes part to the reaction by producing the MS and MSH species at the surface and is regenerated at the end of the catalytic cycle so that it does not appear in the global reaction.

In the same spirit, we have tested several relevant mechanisms for the HDS of 2MT. The elementary step of the model fitting at best experimental results are described here. The first three steps ((E0), (E1) and (E2)) are identical to the mechanism described above for the olefin hydrogenation. The next steps are written as follows:



The adsorption of 2-methylthiophene (labelled as RS) is reported at step (E8). We have considered that the rate determining step corresponds to the hydrogenation of the thiophenic cycle prior to the C–S bond rupture. More precisely, the first hydrogen transfer on the adsorb thiophenic compound (E9) is assumed to be rate determining step. Step (E10) is the second hydrogenation from MH group. Subsequent elementary steps, leading to desulfurized product (alkenes and alkanes) and to the partial regeneration of  $M^*$  sites, occur as reported from step (E11) to (E14). As proposed for olefin hydrogenation step (E7) is proposed to equilibrate the global reaction scheme (full  $M^*$  recovery, avoiding  $H_2S$ -over consumption).

### 2.5.2. Equation rates and Brønsted–Evans–Polanyi relationships

Within the proposed HYDO and HDS mechanisms, the addition of the first hydrogen from the sulfhydryl group is rate determining (steps (E4) and (E9)). Considering both reaction as competitive for the same active sites, the equation of site conservation is modified and written as follows (olefinic compound and thiophenic compound are, respectively, labelled R and RS):

$$\theta^* + \theta_S + \theta_{SH} + \theta_H + \theta_R + \theta_{RS} = 1 \quad (1)$$

Thus, HYDO and HDS reaction rates are, respectively, expressed as:

$$r_{HYDO} = \frac{k_{SH(HYDO)}\theta_{SH}\theta_R}{\alpha_R\alpha_{H_2S}^{1/2}\alpha_S^{1/2}} \quad (2)$$

$$(1 + \alpha_R + \alpha_{RS} + \alpha_S + \alpha_{H_2}\alpha_{H_2S}^{-1/2}\alpha_S^{1/2} + \alpha_{H_2S}^{1/2}\alpha_S^{1/2})^2$$

$$r_{HDS} = \frac{k_{SH(HDS)}\theta_{SH}\theta_{RS}}{\alpha_{RS}\alpha_{H_2S}^{1/2}\alpha_S^{1/2}} \quad (3)$$

$$(1 + \alpha_R + \alpha_{RS} + \alpha_S + \alpha_{H_2}\alpha_{H_2S}^{-1/2}\alpha_S^{1/2} + \alpha_{H_2S}^{1/2}\alpha_S^{1/2})^2$$

$$\text{with } \alpha_i = K_i \frac{P_i}{P^0} \quad \text{and} \quad \alpha_S = \frac{P_{H_2S}}{K_S P_{H_2}} \quad (4)$$

To improve the model fit, an additional term of thermal conversion,  $r_{th}$ , will be added for plotting rate Eqs. (2) and (3). This contribution which is negligible for most of the active systems and does not depend on  $E(\text{MS})$ , accounts for the very low (but different from zero) thermal conversion (appearing at very low or very high  $E(\text{MS})$  non-active catalysts).

In the same spirit as firstly proposed by Kasztelan [36] and more recently revisited by Toulhoat and Raybaud [23], we express the adsorption constant  $K_i$ , and activation energies as a function of a relevant intrinsic parameter of transition metal sulfide catalyst, the sulfur–metal bond energy,  $E(\text{MS})$ . The adsorption constants,  $K_i$ , and the kinetic constant  $k_{SH}$  are thus written as:

$$K_i = e^{\Delta S_i/R - \Delta H_i/RT} = e^{\Delta S_i/R} e^{[\Delta E_{i,0} + \beta_i E(\text{MS})]/RT} \quad (5)$$

$$k_{SH} = \frac{k_B T}{h} e^{-\Delta G^\ddagger/RT} = \frac{k_B T}{h} e^{-[\Delta G_0^\ddagger + \gamma_{SH} E(\text{MS})]/RT} \quad (6)$$

where  $k_B$  and  $h$  are the Boltzmann and Planck's constants, respectively.

### 2.5.3. Identification of the kinetic model and kinetic parameters

If a linear relationship holds between the adsorption energy variation (resp. activation energy) and  $E(\text{MS})$ , resulting from Brønsted–Evans–Polanyi (BEP) relationships [37–39], the  $K_i$  and  $k_{\text{SH}}$  constants depend on the catalyst via  $E(\text{MS})$ . Rate equations are finally a parametrized expression of  $r$  depending on  $T$ ,  $p_{\text{H}_2}$ ,  $p_{\text{H}_2\text{S}}$ . The BEP parameters ( $\Delta E_{i,0}$ ,  $\beta_i$ ) and  $\Delta S_i$  depend on the type of adsorbed molecules,  $i$ , whereas  $\Delta G_0^\ddagger$  and  $\gamma_{\text{SH}}$  depend on the type of reaction. The determination of these kinetic parameters is obtained by minimizing the deviation of the theoretical rates  $r_{\text{HYDO}}$  (Eq. (2)) and  $r_{\text{HDS}}$  (Eq. (3)) from the experimental HYDO and HDS activities measured on the tested catalysts. The numerical values of the fitted parameters  $\Delta G_0^\ddagger$ ,  $\Delta E_{i,0}$ ,  $\beta_i$  and  $\gamma_{\text{SH}}$  are given in Table 3 and will be used in Section 3.3.

Among the one site models [34], we have tested other relevant mechanisms for olefin hydrogenation (HYDO) and 2-methylthiophene HDS. However, the mechanism described previously leads to the models fitting at best HDS and HYDO experimental rates obtained on a FCC gasoline model feed. For the HYDO mechanism, we have verified that assuming a different rate determining step such as (E5) and/or inverting the hydrogenation steps (E4) and (E5) lead to less satisfactory results. For the HDS mechanism, other steps were also assumed for being rate determining. However, all other one site models lead to a larger deviation between theoretical rates and experimental rates, which induces a non-coherent shape and/or position of activity maximum on the volcano.

## 3. Results and discussion

### 3.1. Characterization of the various TMS

The crystalline structure, stoichiometry and specific surface areas of the different TMS and unsupported molybdenum sulfide based catalysts are given, respectively, in Tables 4 and 5.

Table 3  
Numerical values of the fitted kinetic parameters used in adsorption constants (5) and kinetic constant (6)

$\beta_R$	−0.30
$\beta_{\text{RS}}$	−0.49
$\beta_{\text{H}_2}$	0
$\beta_{\text{H}_2\text{S}}$	−1.51
$\beta_S$	−0.61
$\Delta E_R^0$ (kJ/mol)	−29
$\Delta E_{\text{RS}}^0$ (kJ/mol)	−55
$\Delta E_{\text{H}_2}^0$ (kJ/mol)	−120
$\Delta E_{\text{H}_2\text{S}}^0$ (kJ/mol)	+20
$\Delta E_S^0$ (kJ/mol)	−70
$\gamma_{\text{SH}}(\text{HYDO}) = \gamma_{\text{SH}}(\text{HDS})$	0
$\Delta G_{0(\text{HYDO})}^\ddagger$ (kJ/mol)	+59
$\Delta G_{0(\text{HDS})}^\ddagger$ (kJ/mol)	+109

Table 4

Physico-chemical properties of the unsupported monometallic TMS determined by XRD, elemental analysis and specific surface area

Metal (Me)	TMS	S/Me atom	Specific surface area (m <sup>2</sup> /g)
Fe	FeS	0.7	20
Ni	Ni <sub>9</sub> S <sub>8</sub> , NiS	0.9	3
Co	Co <sub>9</sub> S <sub>8</sub>	0.9	22
Pd	PdS	0.8	5
Rh	Rh <sub>2</sub> S <sub>3</sub>	1.7	26
Ru	RuS <sub>2</sub>	1.9	29
Pt	PtS	1.1	29
Mo	MoS <sub>2</sub>	2.2	80

Their composition according to chemical analysis and XRD pattern corresponded to Co<sub>9</sub>S<sub>8</sub>, Rh<sub>2</sub>S<sub>3</sub>, RuS<sub>2</sub>, PtS and MoS<sub>2</sub> [14,28,29]. A mixture of two phases Ni<sub>9</sub>S<sub>8</sub> and NiS was observed for the nickel sulfide. PdS, Co<sub>9</sub>S<sub>8</sub>, Rh<sub>2</sub>S<sub>3</sub>, RuS<sub>2</sub>, PtS have similar specific surface area (around 30 m<sup>2</sup>/g), nickel sulfide and palladium sulfide the lowest (5 m<sup>2</sup>/g) and MoS<sub>2</sub> the highest (80 m<sup>2</sup>/g) (Table 4).

Promoted molybdenum sulfide catalysts by nickel (NiMoS) and cobalt (CoMoS) were also obtained (Table 5) according to chemical analysis and XRD pattern with the desired promoted ratio (around 0.3). The presence of nickel or cobalt decreased strongly the specific surface area from 80 m<sup>2</sup>/g for MoS<sub>2</sub> to 10 m<sup>2</sup>/g for CoMoS and 4 m<sup>2</sup>/g for NiMoS [30]. XPS analysis confirmed the formation of the mixed phases and the promoted ratio.

All the catalysts were characterized after catalytic activity measurements by X-ray diffraction, elemental analysis and XPS in order to show the stability of transition metals sulfides. No modification of structure during the activity measurement can be noticed excepted for nickel sulfides (Ni<sub>9</sub>S<sub>8</sub>, NiS) which were reduced into Ni<sub>3</sub>S<sub>2</sub> sulfide phase.

### 3.2. Transformation of the model feed over sulfide catalysts

The HDS products from the 2MT transformation and the hydrogenation products (HYDO) of 2,3-dimethylbutene (23DMBN) versus residence time are shown, respectively, in Figs. 1 and 2. Rh<sub>2</sub>S<sub>3</sub> was the most active catalyst for the HDS products formation and HYDO products formation. Indeed this corresponds to the highest amount of products (HDS and HYDO) at low residence time. The formation of 2MTHT was also observed with the catalysts having a high hydrogenation activity. MoS<sub>2</sub>, CoMoS, NiMoS and RuS<sub>2</sub> were less active in

Table 5

Physico-chemical properties of the unsupported sulfide molybdenum based catalyst determined by XRD, elemental analysis and specific surface area

Catalyst	Specific surface area (m <sup>2</sup> g <sup>−1</sup> )	S/metal atom	Ni(Co)/ (Ni(Co) + Mo)
MoS <sub>2</sub>	80	2.2	–
CoMoS	10	2.0	0.2
NiMoS	4	2.0	0.2

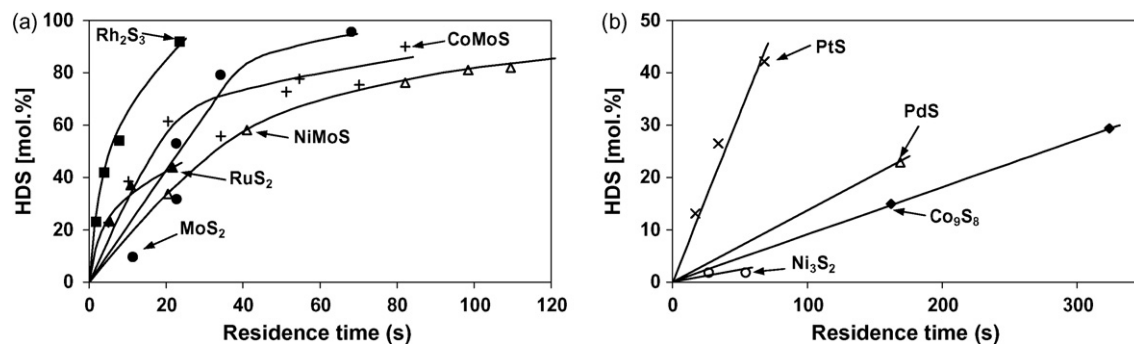


Fig. 1. Transformation of the model feed: 2MT transformation—HDS formation products (as described in Section 2.4) vs. residence time over various unsupported sulfide catalysts: (a)  $\text{Rh}_2\text{S}_3$ ,  $\text{CoMoS}$ ,  $\text{NiMoS}$ ,  $\text{RuS}_2$ ,  $\text{MoS}_2$  and (b)  $\text{Ni}_3\text{S}_2$ ,  $\text{PdS}$ ,  $\text{Co}_9\text{S}_8$ ,  $\text{PtS}$  ( $T = 250^\circ\text{C}$ ,  $P = 20$  bar,  $\text{H}_2/\text{feed} = 360$  l/l). Note: Lines are only guide for the eyes.

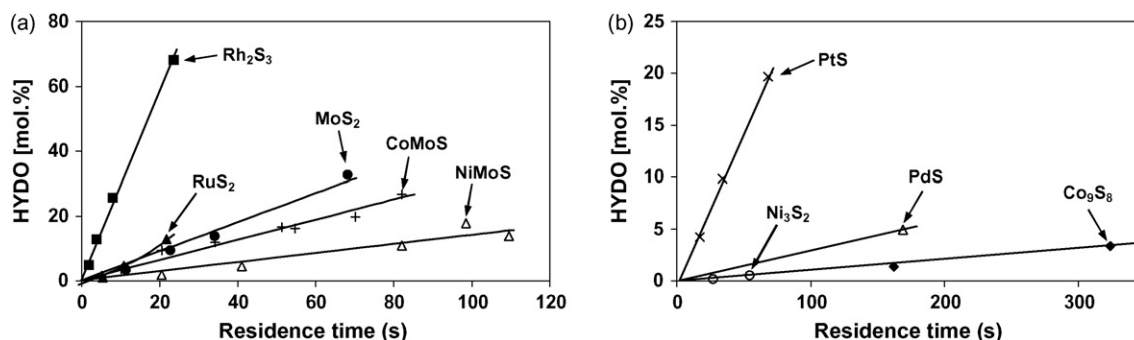


Fig. 2. Transformation of the model feed: 23DMB2N transformation—HYDO formation products (mainly 23DMB, as described in Section 2.4) vs. residence time over various unsupported sulfide catalysts: (a)  $\text{Rh}_2\text{S}_3$ ,  $\text{CoMoS}$ ,  $\text{NiMoS}$ ,  $\text{RuS}_2$ ,  $\text{MoS}_2$  and (b)  $\text{Ni}_3\text{S}_2$ ,  $\text{PdS}$ ,  $\text{Co}_9\text{S}_8$ ,  $\text{PtS}$  ( $T = 250^\circ\text{C}$ ,  $P = 20$  bar,  $\text{H}_2/\text{feed} = 360$  l/l). Note: Lines are only guide for the eyes.

HDS formation and mainly in hydrogenation of 23DMB2N at similar residence time.  $\text{Ni}_3\text{S}_2$  and  $\text{Co}_9\text{S}_8$  were the lowest active catalysts for both reactions (HDS and hydrogenation).  $\text{Rh}_2\text{S}_3$  appeared to be the more selective catalyst for olefins hydrogenation (Fig. 3) and was also the more selective catalyst for the formation of pentane compared to  $\text{RuS}_2$ ,  $\text{MoS}_2$  and the unsupported bimetallic sulfides ( $\text{NiMoS}$  and  $\text{CoMoS}$ ) (Fig. 4). The selectivity towards pentane/pentane + pentene was stable whatever the level of HDS except for the unsupported bimetallic sulfides (Fig. 4). The results are not reported for nickel sulfide catalyst since very low HDS conversion is observed (Fig. 1b). For both mixed sulfide catalysts an increase of the selectivity was observed corresponding to an increase of

the formation of pentane for the highest level of HDS. These results suggests that the hydrogenation of alkenes was disfavored in the presence of 2MT as a result of an adsorption competition of the various compounds on the catalyst surface. In this case, the unsupported bimetallic sulfides ( $\text{NiMoS}$  and  $\text{CoMoS}$ ) were more sensitive than the unsupported monometallic transition metals.

The change of the formation of hydrogenation products from 23DMB2N confirmed that the hydrogenation was first slow down at low HDS level and favored when the HDS level increased. The discriminating parameter, which can be used to evaluate the performances of the catalysts regarding the HDS of FCC gasoline is the HDS/HYDO selectivity (Fig. 5). From this

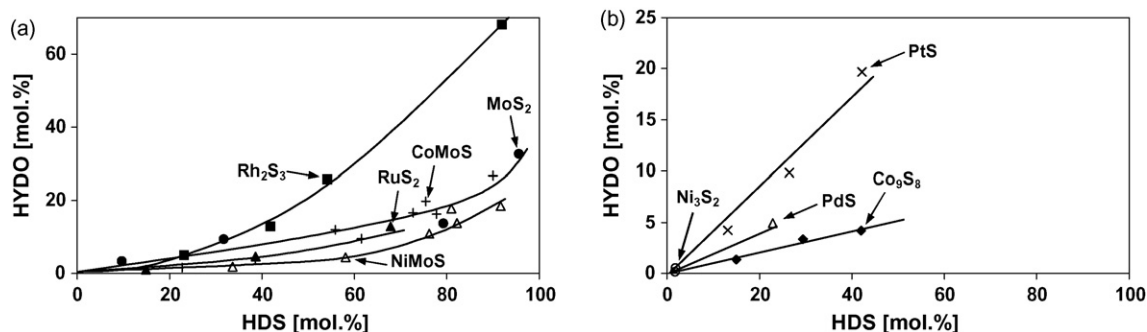


Fig. 3. Transformation of the model feed: 23DMB2N transformation—HYDO formation products (23DMB) vs. HDS yield over various unsupported sulfide catalysts (a)  $\text{Rh}_2\text{S}_3$ ,  $\text{CoMoS}$ ,  $\text{NiMoS}$ ,  $\text{RuS}_2$ ,  $\text{MoS}_2$  and (b)  $\text{Ni}_3\text{S}_2$ ,  $\text{PdS}$ ,  $\text{Co}_9\text{S}_8$ ,  $\text{PtS}$  ( $T = 250^\circ\text{C}$ ,  $P = 20$  bar,  $\text{H}_2/\text{feed} = 360$  l/l). Note: Lines are only guide for the eyes.

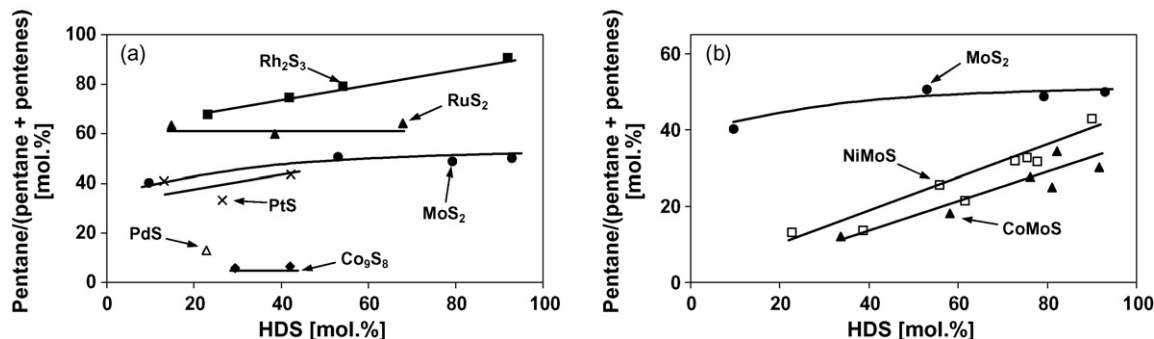


Fig. 4. Transformation of the model feed: 2MT transformation. Selectivity towards pentane (pentane/pentane + pentenes) vs. HDS yield over various unsupported sulfide catalysts (a) Rh<sub>2</sub>S<sub>3</sub>, CoMoS, NiMoS, RuS<sub>2</sub>, MoS<sub>2</sub> and (b) Ni<sub>3</sub>S<sub>2</sub>, PdS, Co<sub>9</sub>S<sub>8</sub>, PtS ( $T = 250\text{ }^{\circ}\text{C}$ ,  $P = 20\text{ bar}$ ,  $\text{H}_2/\text{feed} = 360\text{ l/l}$ ). Note: Lines are only guide for the eyes.

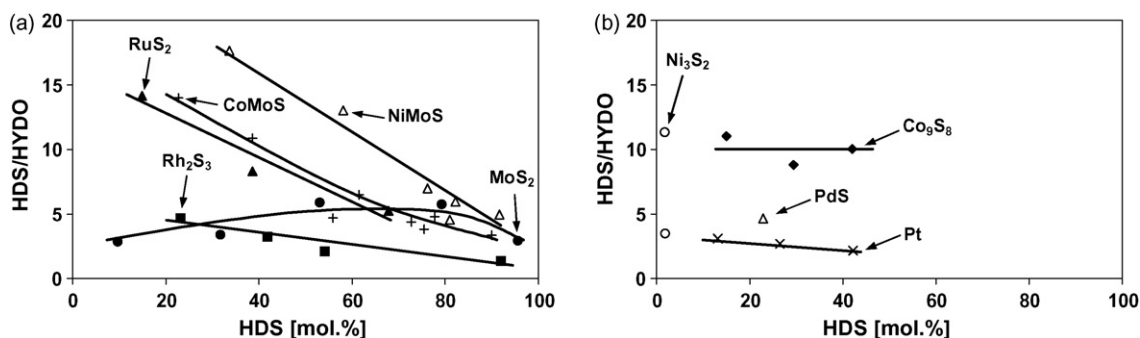


Fig. 5. Transformation of the model feed: HDS/hydrogenation selectivity (HDS/HYDO) of the hydrotreating process vs. HDS yield over (a) Rh<sub>2</sub>S<sub>3</sub>, CoMoS, NiMoS, RuS<sub>2</sub>, MoS<sub>2</sub> and (b) Ni<sub>3</sub>S<sub>2</sub>, PdS, Co<sub>9</sub>S<sub>8</sub>, PtS ( $T = 250\text{ }^{\circ}\text{C}$ ,  $P = 20\text{ bar}$ ,  $\text{H}_2/\text{feed} = 360\text{ l/l}$ ). Note: Lines are only guide for the eyes.

point of view, the selectivity for all of the catalysts decreased when the HDS level increased. The best catalyst was the unsupported NiMoS catalyst at low and medium HDS level and the selectivity became similar for various catalysts (NiMoS, CoMoS and MoS<sub>2</sub>) at high HDS level (near 90%) (Fig. 5).

### 3.3. HDS and HYDO activities versus $E(\text{MS})$ and microkinetic interpretation

Volcano type relationships between the ab initio calculated metal–sulfur bond energies  $E(\text{MS})$  and the activity in the

hydrodesulfurization of 2MT (HDS) on the one hand, and the hydrogenation of 23DMB2N (HYDO) on the other, were obtained. The lowest activities corresponded to Ni<sub>3</sub>S<sub>2</sub> which had the lowest  $E(\text{MS})$  and to MoS<sub>2</sub> which had the highest  $E(\text{M-S})$ . The maximum in the activity was obtained with Rh<sub>2</sub>S<sub>3</sub>, which have an intermediate  $E(\text{M-S})$  (Figs. 6 and 7).

The BEP linear relationships used, for the kinetic modelling of HYDO and HDS reactions are plotted in Fig. 8. All adsorptions are exothermic. The higher  $E(\text{MS})$ , the stronger the interaction of the active free site  $\text{M}^*$  with 23DMB2N, 2MT,  $-\text{S}$ ,  $-\text{SH}$  is.

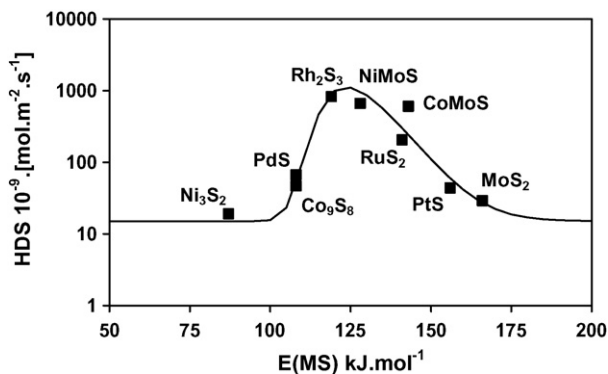


Fig. 6. Hydrodesulfurization of 2MT—comparison between experimental results and kinetic model (black line) plotted against sulfur–metal bond energies,  $E(\text{MS})$  ( $T = 250\text{ }^{\circ}\text{C}$ ,  $P = 20\text{ bar}$ ,  $\text{H}_2/\text{feed} = 360\text{ l/l}$ ).

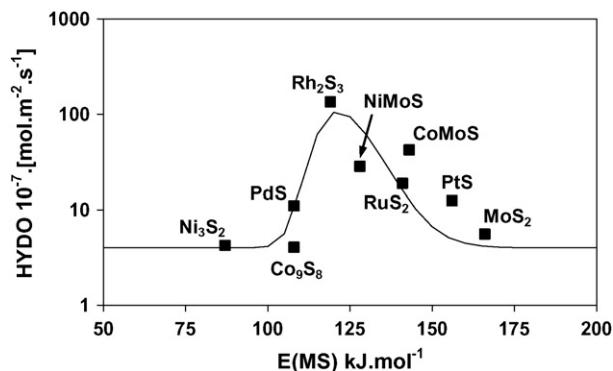


Fig. 7. Hydrogenation of 23DMB2N—comparison between experimental results and kinetic model (black line) considering HYDO and HDS reaction simultaneously plotted against sulfur–metal bond energies,  $E(\text{MS})$  ( $T = 250\text{ }^{\circ}\text{C}$ ,  $P = 20\text{ bar}$ ,  $\text{H}_2/\text{feed} = 360\text{ l/l}$ ).



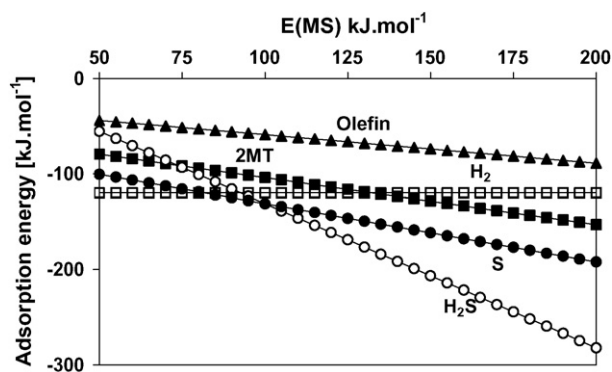


Fig. 8. Linear BEP relationships between adsorption energies (and activation energies) and the sulfur–metal bond energies,  $E(\text{MS})$ .

We underline that the relevant insights in Fig. 8 are the relative positions and slopes of the BEP relationships for all reactants with respect to  $\text{H}_2$ . Indeed, it would be (formally) possible to choose a fitted BEP parameter corresponding to a linear variation of adsorption energy of  $\text{H}_2$  with  $E(\text{MS})$ . This different choice would imply a shift of the BEP relationship slopes for all other reactants. However, the shape and position described in what follows and deduced from the relative position of the BEP relationships would remain unchanged.

In Figs. 6 and 7, it can be observed that the volcano curves as already proposed for toluene hydrogenation [26] and DBT HDS [23] are recovered for 23DMB2N hydrogenation and for 2MT HDS, respectively.

For both HYDO and HDS activities, we find that the optimal catalysts ( $\text{Rh}_2\text{S}_3$ , NiMoS and CoMoS) are found for intermediate value of  $E(\text{MS})$  on the Sabatier principle [22]. The volcano shape is still present even if we consider HYDO and HDS as simultaneous reaction (e.g. at the same active sites).

As reported in prior work [26,27], a careful analysis of the species coverage as a function of the  $E(\text{MS})$  (Fig. 9) reveals that for high  $E(\text{MS})$  the surface is saturated by MSH species. For low  $E(\text{MS})$ , the surface is fully covered by MH species. These two extreme regions correspond to very low number of 23DMB2N and 2MT molecules adsorbed on the surface and the HYDO and HDS rate law decrease abruptly (as expected from the rate laws (1) and (2) the rates decrease when  $\theta_{\text{R}}$  or  $\theta_{\text{RS}}$  value is low at high and low  $E(\text{MS})$ ). For intermediate  $E(\text{MS})$ , the

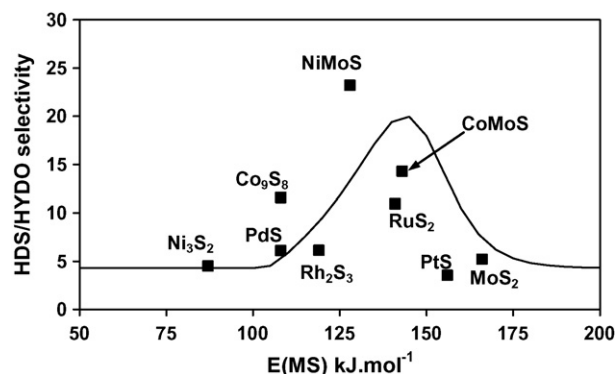


Fig. 10. Selectivity HDS/HYDO—comparison between experimental results and kinetic model (black line) considering HYDO and HDS reaction simultaneously plotted against sulfur–metal bond energies,  $E(\text{MS})$  ( $T = 250^\circ\text{C}$ ,  $P = 20$  bar,  $\text{H}_2/\text{feed} = 360$  l/l).

23DMB2N and 2MT coverage reaches a maximum. Furthermore, the sulfhydryl species coverage is simultaneously high at the surface which maximizes the product  $\theta_{\text{reactant}} \times \theta_{\text{SH}}$  (reactant = R or RS) and explain why the both maximum of HDS and HYDO are obtained for intermediate  $E(\text{MS})$  value. It must be noticed that the coverage of the sulfur compound is larger than the one of the olefin which characterizes the inhibitor property of the methyl-thiophene for olefin.

From this model, considering HDS and HYDO reaction simultaneously, we have determined the theoretical selectivity HDS/HYDO obtained from the ratio of HDS and HYDO rate laws (Eqs. (2) and (3), respectively) as a function of the sulfur–metal bond energy (Fig. 10, HDS around 40%). Regarding the experimental HDS/HYDO selectivity, the best catalysts would be NiMoS with an intermediate  $E(\text{MS})$  of 130 kJ/mol. We observe that the selectivity shape obtained correlates qualitatively with the experimental selectivity trend. Even if, the theoretical selectivity optimum is shifted to higher  $E(\text{MS})$  compare to experimental values and the amplitude is slightly slower, an optimal selectivity is pointed out at intermediate  $E(\text{MS})$  value from this model. The position of the maximum depends on the relative position of HDS and HYDO maximal activities. In particular, it can be observed that position of the HDS maximum is located at higher  $E(\text{MS})$  than the position of HYDO.

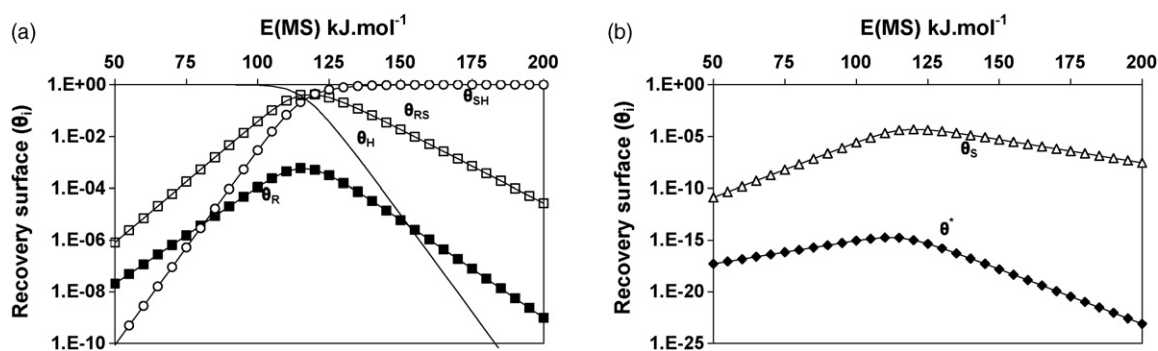


Fig. 9. Surface coverage of the predominant species as a function of  $E(\text{MS})$ , deduced from the kinetic model: (a) most predominant species: 23DMB2N ( $\theta_{\text{R}}$ ), 2MT ( $\theta_{\text{RS}}$ ), MSH ( $\theta_{\text{SH}}$ ) and MH ( $\theta_{\text{H}}$ ) and (b) less predominant species:  $\text{M}^*$  ( $\theta^*$ ) and MS ( $\theta_{\text{S}}$ ). Numerical values of BEP parameters are reported in Table 3.

#### 4. Conclusion

We can conclude that it is possible to generalize the volcano curve relationship between the *ab initio* calculated metal–sulfur bond energy ( $E(\text{MS})$ ) of the various unsupported transition monometallic sulfides (TMS) and bimetallic sulfides (NiMoS and CoMoS) and their activity to the HDS of alkylthiophenes such as 2MT and hydrogenation of olefins such as 23DMB2N under conditions typical of the selective HDS of FCC gasoline. In particular,  $\text{Rh}_2\text{S}_3$  with an intermediate sulfur–metal bond energy of 119 kJ/mol was the most active catalyst for the hydrogenation and HDS. These results are consistent with the Sabatier principle where intermediate  $E(\text{MS})$  values correspond to optimal surface distribution of active species. It also extends the volcano curve's concept established for the model olefin molecule [27] to a model FCC gasoline feed, where HDS and HYDO reactions are taking place simultaneously.

Furthermore, the HDS/HYDO selectivity which is the most important parameter in the deep HDS of gasoline, reveals also a volcano curve relationship as a function of  $E(\text{MS})$  with the maximum obtained with the unsupported bimetallic NiMoS catalyst. Among several relevant microkinetic models tested, the best fit of the reaction rates and selectivities is obtained by considering a one site model within the Langmuir–Hinshelwood formalism. The (heterolytic type) dissociation of  $\text{H}_2\text{S}$  (or  $\text{H}_2$ ) takes place on MS species and free  $\text{M}^*$  sites, while the competitive adsorption of the sulfur molecule and alkene occurs on  $\text{M}^*$  site. The model recovers the optimum of HDS/HYDO selectivity for intermediate  $E(\text{MS})$  which opens new routes for a rational improvement of the selectivity of hydrotreatment catalysts.

#### Acknowledgements

A. Daudin thanks I.F.P. and CNRS for a Ph.D. grant. The authors also thank P. Lecour and C. Legens for XPS analysis (IFP Lyon) and for the fruitful discussions.

#### References

- [1] Official Journal of the European Union, L76 (2003) 10.
- [2] S. Hatanaka, M. Yamada, O. Sadakane, *Ind. Eng. Chem. Res.* 36 (1997) 1519.
- [3] S. Hatanaka, M. Yamada, O. Sadakane, *Ind. Eng. Chem. Res.* 36 (1997) 5110.
- [4] S. Hatanaka, M. Yamada, O. Sadakane, *Ind. Eng. Chem. Res.* 37 (1998) 1748.
- [5] S. Brunet, D. Mey, G. Pérot, C. Bouchy, F. Diehl, *Appl. Catal. A: Gen.* 278 (2005) 143.
- [6] D. Mey, S. Brunet, C. Canaff, F. Maugé, C. Bouchy, F. Diehl, *J. Catal.* 227 (2004) 436.
- [7] J.T. Miller, W.J. Reagan, J.A. Kaduck, J. Kropf, *J. Catal.* 193 (2000) 123.
- [8] C. Sudhakar, M.R. Cesar, R.A. Heinrich, US Patent 5,525,211, Texaco, 1996.
- [9] P.S.E. Dai, D.E. Sherwood Jr., R.H. Petty, US Patent 5,340,466, Texaco, 1994.
- [10] O. Sadakane, EP 0 745 660 A1, Mitsubishi Oil Corporation, 1996.
- [11] S. Hatanaka, *Catal. Surv. Asia* 9 (2005) 87.
- [12] S. Hatanaka, O. Sadakane, US Patent 6,120,679, Mitsubishi Oil Corporation, 2000.
- [13] H. Topsøe, B.S. Clausen, F.E. Massoth, in: J.R. Anderson, M. Boudard (Eds.), *Hydrotreating Catalysis, Science and Technology*, Springer Verlag Press, Berlin, 1996, p. 1.
- [14] T.A. Pecoraro, R.R. Chianelli, *J. Catal.* 67 (1981) 430.
- [15] M. Lacroix, H. Marrakchi, C. Calais, M. Breysse, C. Forquy, *Stud. Surf. Sci. Catal.* 59 (1991) 277.
- [16] J.P.R. Vissers, C.K. Groot, E.M. VanOers, V.H.J. de Beer, R. Prins, *Bull. Soc. Chim. Belg.* 93 (1984) 813.
- [17] M.J. Ledoux, O. Michaux, J. Agostini, P. Panissod, *J. Catal.* 102 (1986) 275.
- [18] P. Raybaud, *Appl. Catal. A: Gen.* 322 (2007) 76.
- [19] R.R. Chianelli, G. Berhault, P. Raybaud, S. Kasztelan, J. Hafner, H. Toulhoat, *Appl. Catal. A: Gen.* 227 (2002) 83.
- [20] P. Raybaud, J. Hafner, G. Kresse, H. Toulhoat, *J. Phys.: Condens. Matter* 9 (1997) 11107.
- [21] H. Toulhoat, P. Raybaud, S. Kasztelan, G. Kresse, J. Hafner, *Catal. Today* 50 (1999) 629.
- [22] P. Sabatier, *Berichte der Deutschen Chem. Gesellschaft* 44 (1911) 2001.
- [23] H. Toulhoat, P. Raybaud, *J. Catal.* 216 (2003) 63.
- [24] M. Lacroix, N. Boutarfa, C. Guillard, M. Vrinat, M. Breysse, *J. Catal.* 120 (1989) 473.
- [25] N. Guernalec, T. Cseri, P. Raybaud, C. Geantet, M. Vrinat, *Catal. Today* 98 (2004) 61.
- [26] N. Guernalec, C. Geantet, P. Raybaud, M. Aouine, T. Cseri, M. Vrinat, *Oil Gas Sci. Technol. Rev. IFP* 61 (2006) 515.
- [27] A. Daudin, S. Brunet, G. Perot, P. Raybaud, C. Bouchy, *J. Catal.* 248 (2007) 111.
- [28] G. Berhault, A. Mehta, A.C. Pavel, J. Yang, L. Redon, M.J. Yacaman, L.C. Araiza, A.D. Moller, R.R. Chianelli, *J. Catal.* 198 (2001) 9.
- [29] Y. Iwata, K. Sato, T. Yoneda, Y. Miki, Y. Sugimoto, A. Nishijima, H. Shimada, *Catal. Today* 45 (1998) 353.
- [30] S. Fuentes, G. Diaz, F. Fedraza, H. Rojas, N. Rosas, *J. Catal.* 113 (1988) 535.
- [31] C.D. Wagner, W.M. Riggs, L.E. Davis, J.F. Moulder, in: G.E. Muilenberg (Ed.), *Handbook of X-ray Photoelectron Spectroscopy*, Perkin-Elmer Corporation (Physical Electronics), 1979.
- [32] M. Guisnet, P. Canesson, R. Maurel, *Bull. Soc. Chim. Fr.* 10 (1970) 3566.
- [33] S. Kasztelan, *Hydrotreating Technology for Pollution Control*, Marcel Dekker Inc., New York, 1996, pp. 29–45.
- [34] S. Kasztelan, D. Guillaume, *Ind. Eng. Chem. Res.* 33 (1994) 203; S. Kasztelan, D. Guillaume, *Ind. Eng. Chem. Res.* 34 (1995) 1500.
- [35] P. Raybaud, J. Hafner, G. Kresse, S. Kasztelan, H. Toulhoat, *J. Catal.* 189 (2000) 129.
- [36] S. Kasztelan, *Appl. Catal. A: Gen.* 83 (1992) L1.
- [37] J.N. Brønsted, K.J. Pedersen, *Z. Phys. Chem.* 108 (1924) 185.
- [38] M.G. Evans, M. Polanyi, *Trans. Faraday Soc.* 32 (1936) 1333.
- [39] M.G. Evans, M. Polanyi, *Trans. Faraday Soc.* 11 (1938) 34.